

A new setup for high resolution fast X-ray reflectivity data acquisition


Milena Lippmann, Adeline Buffet, Kathrin Pflaum, Anita Ehnes, Anca Ciobanu, and Oliver H. Seeck

Citation: [Review of Scientific Instruments](#) **87**, 113904 (2016); doi: 10.1063/1.4967239

View online: <http://dx.doi.org/10.1063/1.4967239>

View Table of Contents: <http://aip.scitation.org/toc/rsi/87/11>

Published by the [American Institute of Physics](#)



Small Conferences. BIG Ideas.

Applied Physics
Reviews

SAVE THE DATE!
3D Bioprinting: Physical and Chemical Processes
May 2–3, 2017 • Winston Salem, NC, USA

A new setup for high resolution fast X-ray reflectivity data acquisition

Milena Lippmann,¹ Adeline Buffet,¹ Kathrin Pflaum,² Anita Ehnes,¹ Anca Ciobanu,¹ and Oliver H. Seeck¹

¹Deutsches Elektronen-Synchrotron DESY, Notkestraße 85, 22607 Hamburg, Germany

²Max-Planck-Institute for Solid State Research, Heisenbergstraße 1, 70569 Stuttgart, Germany

(Received 5 July 2016; accepted 24 October 2016; published online 11 November 2016)

A new method for fast x-ray reflectivity data acquisition is presented. The method is based on a fast rotating, slightly tilted sample reflecting to a stationary mounted position sensitive detector and it allows for measurements of reflectivity curves in a quarter of a second. The resolution in q -space mainly depends on the beam properties and the pixel size of the detector. Maximum q_z -value of 1 \AA^{-1} can be achieved. The time-temperature depending structure changes of poly(N -isopropylacrylamide) thin films were investigated *in situ* by applying the fast-reflectivity setup. The results are presented in this paper as illustration of the method and proof of principle. *Published by AIP Publishing.* [<http://dx.doi.org/10.1063/1.4967239>]

INTRODUCTION

X-ray reflectivity (XRR) is a non-destructive technique used in biology, chemistry, physics, and materials science to characterize surfaces, thin films (from sub-nm up to 500 nm), and multilayers.^{1–4} In particular, parameters such as thickness, interface roughness, and layer density can be obtained with accuracies of better than 0.1 nm in thickness and roughness, and 5% in density calculation. In the majority of cases, x-ray reflectivity of solid samples is acquired by performing $\theta/2\theta$ angular scans. In this case, a monochromatic x-ray beam is used while both the sample (θ) and the detector (2θ) are scanned stepwise. To determine the film parameters accurately, the angular resolution of the scan should be high (small step width) and the q -range large where q is the wave vector transfer which directly depends on θ with $q = 4\pi \sin \theta / \lambda$, where λ is the wavelength of the X-rays.

As to its high sensitivity in the characterization of thin films, XRR is a well-established method for *in situ* investigations of dynamic phenomena such as the growth of thin films, polymerization processes, protein adsorption, interdiffusion, and annealing processes in multi-layer systems. However, up to now the time resolution achieved is strongly limited by the data acquisition method itself: The $\theta/2\theta$ scans imply accelerating, decelerating, and backslashing of the scanned motors as well as movements in forth and back directions which prevent from a continuous capture of the reflectivity data. Also attenuators, which protect detector against beam damages, have to be moved frequently due to the high dynamic range of reflectivity curves. Typical time resolutions of the order of a few minutes have been achieved for reflectivity in a q -range of $0\text{--}0.5 \text{ \AA}^{-1}$.^{5–7} The procedure can significantly be accelerated by using on-the-fly scans and fast attenuators as used at the SOLEIL beamline SIXS.⁸ Instead of scanning 2θ it is possible to use a position sensitive detector and only scan the incident angle θ . Still drawbacks of the stepwise scanning of the incident angle discriminate the use of this method for *in situ* studies. Alternative approaches exist. One is to use a white x-ray beam and an energy dispersive

detector.^{9–12} However, the heat load on the sample due to the white beam is tremendous and samples can easily be damaged. Furthermore x-ray sources such as x-ray tubes and undulator sources cannot deliver high-intensity white beams with uniform energy distribution of the photons. Finally, the time resolution and q -resolution are strongly limited by the energy resolution and the dynamic range of the detector.^{9–12} Another approach is to generate a strongly focused x-ray beam and to make use of the divergence of the beam for an angular dispersive reflectivity.¹³ Here the q -space and resolution are restricted by the maximum opening angle of the focused beam. Also the strong focusing means high flux density at the sample, which is not advantageous for polymer or biological samples.¹⁴

In this work, we propose a new method for fast x-ray reflectivity data acquisition. In the example chosen to illustrate the application of the new method, we recorded the data with a time resolution of 2 s and a maximum q of 0.55 \AA^{-1} . Better time resolutions (down to a quarter of a second) are achievable, depending on the piezo rotation stage speed, the photon flux, and the detector. The time-temperature structure changes of poly(N -isopropylacrylamide) (pNIPAM) thin films were measured by this method and are presented here. Similar studies have been done by Wang *et al.* The authors used neutron reflectivity measurements (time-of-flight) where the shortest acquisition time was 14 s (10 s data acquisition time and 4 s data read-out time) in a q -range of $0\text{--}0.08 \text{ \AA}^{-1}$.^{15,16}

EXPERIMENTAL SETUP, DATA ACQUISITION, AND DATA PROCESSING

This section is meant as an overview. Details and actual parameters of the setup are listed in the section titled Time-temperature structure dependence of pNIPAM thin films.

The fast reflectivity method presented in this work employs a stationary mounted position sensitive detector and generates the incident angle θ by means of rotation of a specially designed sample holder. A moderately focused

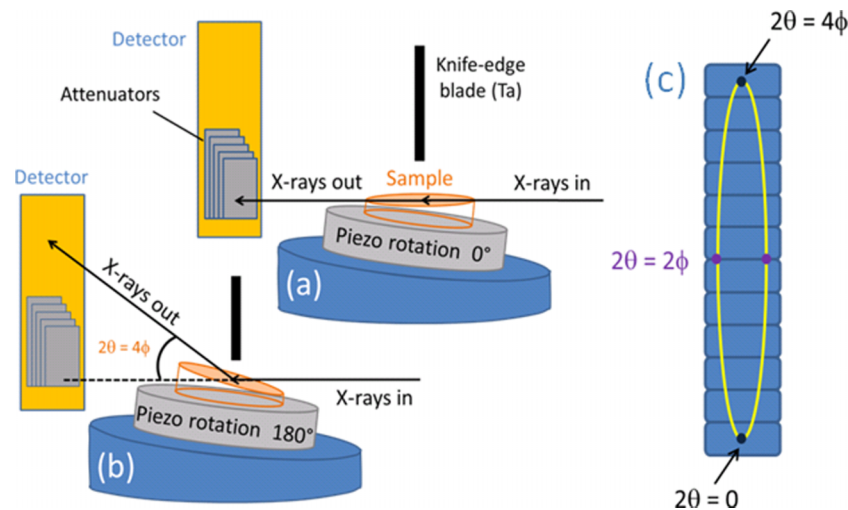


FIG. 1. Left: Schematic view of the setup. (a) Piezo rotation = 0° , $\theta = 0^\circ$. (b) Piezo rotation = 180° , $\theta = 2\phi$. (c) The specular reflected beam describes kind of an ellipse on the detector sensitive area.

x-ray beam travels horizontally with respect to the sample. The sample holder consists of a bias cut cylinder, which is mounted on a wobble-free piezo-driven rotation (see Fig. 1(a)). The construction is mounted on a conventional goniometer tilting stage. The angle ϕ defined by the bias cut of the cylinder is compensated by the goniometer tilting stage of the diffractometer at the initial position such that the sample is aligned parallel to the primary beam. Furthermore the primary beam hits the lower part of the detector. The beam is reflected to the upper direction on rotating the piezo. The angle of the beam reflected by the sample to the detector changes from 0 to 4ϕ , while the incident angle changes from 0 to 2ϕ (see Fig. 1(b)). The reflected beam would move on a 2D area detector with a trajectory similar to a narrow vertical ellipse. However, for this experiment we used a horizontally integrating 1D-detector (see Fig. 1(c)). One complete reflectivity curve is recorded by rotating the piezo stage from 0 to 180° . Fast data acquisition is performed while the piezo drive is rotating at a frequency of 0.1–2 Hz. The angular resolution is mainly depending on the beam properties and the detector pixel size.

Since the intensity of a reflectivity scan varies over several orders of magnitude when varying the incident angle, a set of attenuators of different thicknesses in front of the detector is mandatory. In our test experiments, we used Fe and Ag thin foils. The number and positions of the foils have to be optimized with a sample similar to the studied one prior to the *in situ* experiment. The foil adjustment depends on the particular configuration (sample, energy, and detector). For this slit-less setup, the contribution of background signal is significant; therefore, a knife-edge blade (Ta) is placed just above the sample to suppress unwanted air scattering. However this was not sufficient to reduce the strong background signal at higher q -values. The exposure time for the data acquisition is a critical parameter: at long exposure times, the diffuse scattering from the sample at low θ creates strong background signals at larger θ and floods the detector at the reflection position for large θ (see Fig. 2). Therefore, the complete reflectivity has to be recorded using several

frames of short exposure times (here typically 0.05–0.1 s). The useful signal in one frame consequently spans only a small angular range where the specular reflected beam appears. The higher background contribution at smaller incident angles can easily be observed in the figure, at channels <600 where no attenuators are used. The appropriate frame exposure time depends of the piezo-rotation speed. For a quarter turn per second (0.25 Hz), the exposure time 0.05 s was working well. A systematic study of the piezo rotation speed versus the detector exposure time has to be done before the actual experiment.

A Matlab script was used to generate the complete reflectivity curves from the frame sets with short exposure times. The algorithm is based on the following steps: (1) Raw data frames corresponding to certain reflectivity curves are separated. We call them Reflectivity Data Set Frames (RDSFs). (2) The attenuation correction is performed on the RDSFs, the useful signal from one RDSF is extracted

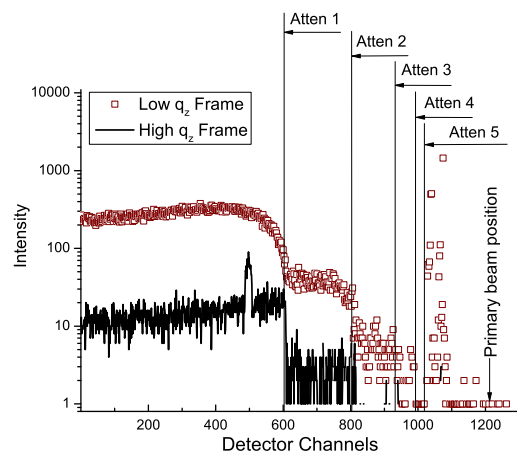


FIG. 2. Two data frames with acquisition time of 0.1 s and rotation speed of 45° per second are shown: Low q_z -frame and high q_z -frame from the low q_z - and high q_z -range of the RDSF, respectively. The Low q_z -frame has a useful signal from 1034 to 1096 channels and the high q_z -Frame from 485 to 509 channels. The position of the attenuator foils is indicated by the lines.

manually, and a template is created in which the useful angular range for each frame of the reflectivity data set is stored. This template is applied to the rest of the RDSFs. (3) The template also accounts for the fact that the lower and top parts of the trajectory per channel are illuminated longer than the left and right side parts. The script consists of several macros that have to be run one after another and still no user friendly environment exists.

TIME-TEMPERATURE STRUCTURE DEPENDENCE OF pNIPAM THIN FILMS

The sample pNIPAM belongs to the class of Lower Critical Solution Temperature (LCST) polymers and it undergoes a hydrophilic/hydrophobic transition at roughly 32 °C in solution.¹⁷ The transition in polymer films implies a reduction of the film thickness with temperature increase above the LCST. The transition temperature in case of pNIPAM thin films is expected to be also 32 °C. The effect is stronger when the samples are swollen after preparation.¹⁵ In the current example, the samples were used as prepared and only the residual water from the preparation procedure was present in the film. However, a reduction of the film thickness with the temperature change could be observed with a time resolution of 2 s per reflectivity.

The films were spin-coated from polymer solution prepared according to the recipe for spin-coated samples given in Ref. 18. The measurement of the reflectivity curves in dependence of the time and temperature was performed at the high resolution diffraction beamline P08 situated at the 3rd generation synchrotron radiation source PETRA III at DESY.¹⁹ The beam size was $(30 \times 300) \mu\text{m}^2$ (V \times H) at photon energy of 18 keV. The accessible maximum q -value depends on the bias cut angle ϕ and the x-ray energy. Using a cylinder with a bias cut angle $\phi = 0.875^\circ$, a maximum q of 0.55 \AA^{-1} was achieved. The machining of the bias cut angle cannot be done more precise than 0.05° , the gluing of the sample by a very thin adhesive layer results into another uncertainty of maximum 0.1° . Therefore, the possible loss in bias cut angle is maximum 20% of the originally selected value which should be taken into account when cutting the bias angle. In any case, by changing the photon energy the maximum q -value can additionally be tuned. For all these reasons, the actual bias cut angle has to be determined for each sample by measuring the angle of the reflected beam versus the azimuth angle ϕ , a very quick procedure. The exact value of ϕ is one of the parameters needed in the Matlab script. The distance sample detector was 470 mm. A Mythen strip detector (Dectris) with 1280 pixels at $50 \mu\text{m}$ height and a frame rate of 0.05 s was used. The Mythen detector works without dead time or interruption between frames. The piezo stage was rotating with a quarter turn per second (0.25 Hz) so one reflectivity curve was recorded in 2 s. The actual set of data was recorded as follows: While the temperature was increased from room temperature to 42 °C, the temperature vs. time curve was recorded and the reflectivity curves were measured. A total of 330 reflectivity curves were measured in 11 records (30 reflectivity curves/record). Taking into account

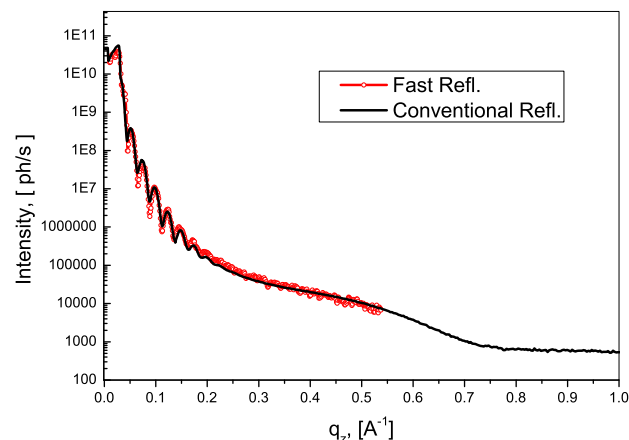


FIG. 3. Fast reflectivity curve (line with circle) obtained in 2 s vs. conventional reflectivity curve (continuous black line) obtained for the same sample in ca. 20 min.

the rotation speed of the piezo stage and the frame duration (0.05 s), one reflectivity curve consists of 40 frames. The time gaps in Fig. 5 are the breaks between the records. It should be mentioned that these time gaps are artificial and can easily be avoided by counting more frames. However, in the examples presented here, the time gaps are not of importance. In general, the acquisition parameters (such as the piezo rotation speed and the frame time) should always be optimized according to the time constants of the studied process. In Fig. 3, one of the reconstructed fast reflectivity curves is compared with a conventionally recorded reflectivity curve (where the sample (θ) and the detector (2θ) are scanned stepwise) of the same sample.

The recorded data were fitted using the Parratt recursive formalism. The electron density profile in the direction perpendicular to the substrate was modeled by three layers (see Fig. 4). The first layer represents the silicon oxide layer on top of the silicon wafer. The polymer film is modeled as the superposition of two layers. The attempt to simulate the polymer film as one layer did not yield satisfactory results; therefore, a two-layer model was applied. The following arguments could legitimate the modelling of the polymer film with two layers: It is well-established that the surface influences the chain conformation resulting in closer molecular packing and higher electron density in the vicinity of the surface. Moreover, some authors report that pNIPAM films store different amount of water in the depth of the polymer film leading to difference of the electron density in the depth profile.¹⁷

The polymer layer close to the substrate was denoted as “Poly1” and the top polymer layer as “Poly2.” It was supposed that the temperature change in the range of 27°–42° does not affect the thickness and roughness of the silicon oxide layer and the substrate. The roughness of the silicon substrate was fixed to 9.71 \AA . The thickness, the roughness, and the dispersion (the dispersion, δ is connected to the electron density of the material through the equation $\delta = r_e \rho \lambda^2 / (2\pi)$, where r_e is the classical electron radius and ρ the electron density.) of the silicon oxide layer were fixed to 20 \AA , 1.23 \AA and 1.10×10^{-6} , respectively, as achieved by a refinement

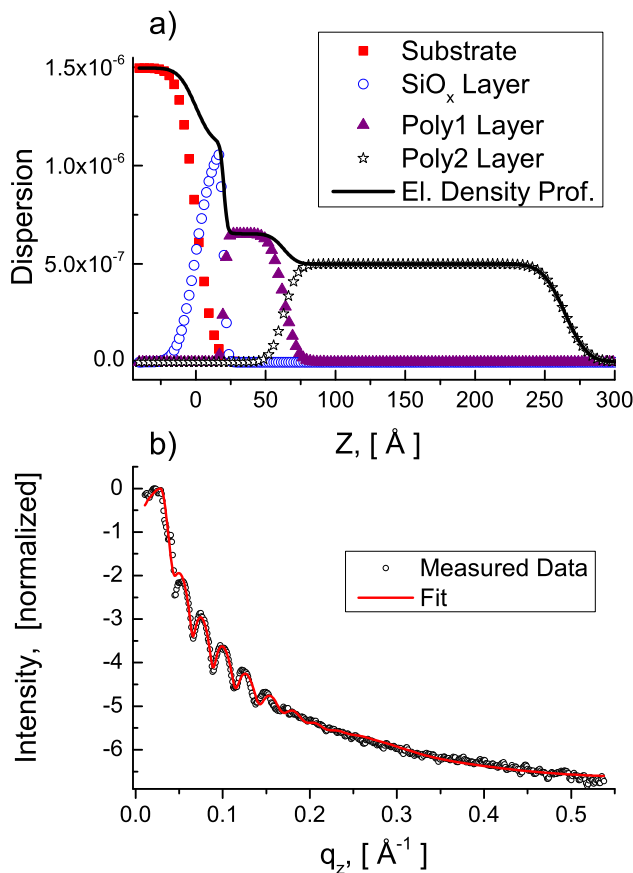


FIG. 4. (a) The dispersion of the three layers and the substrate. The superposition of the supposed layer structure and substrate defines the electron density profile in the direction “z” perpendicular to the surfaces. (b) Measured reflectivity curve at $t = 0$ and corresponding simulated curve according to our model.

of the first reflectivity curve (recorded at $t = 0$). Only the parameters (thickness, roughness, and dispersion) of the Poly1 and Poly2 layers were refined to fit the morphological changes following the time-temperature curve. Fig. 5 presents the results from the data processing. The morphological changes can be classified into two regimes corresponding to the two different temperature regimes observed. In the first part, when the temperature increases linearly with the time ($t < 100$ s), the thickness of the Poly2 layer decreases with the rate of $4.5 \times 10^{-2} \text{ \AA/s}$. Moreover the roughness of the Poly2 layer and the dispersion of both layers slightly rise (see Figs. 5(b) and 5(c)). In the second regime ($t > 100$ s) where the temperature is about 42°C , the Poly2 layer thickness shrinks at a rate of $6.5 \times 10^{-3} \text{ \AA/s}$. The thickness and roughness of the Poly1 layer remain more or less constant. The mean values of the thickness and roughness of the Poly1 layer are 40 \AA and 8.5 \AA respectively. The behavior in the second regime suggests annealing of the polymer film.

The theoretical dispersion value of the pNIPAM at 18 keV is 0.766×10^{-6} . The dispersion of the Poly1 layer with a mean value of 0.7110×10^{-6} agrees well with the theoretical value. The dispersion of Poly2 layer has a mean value of 0.50×10^{-6} which is evidence that the molecular chains in the Poly2 layer have larger excluded volume in comparison to that of the Poly1 layer. Despite the fact that the data significantly spread,

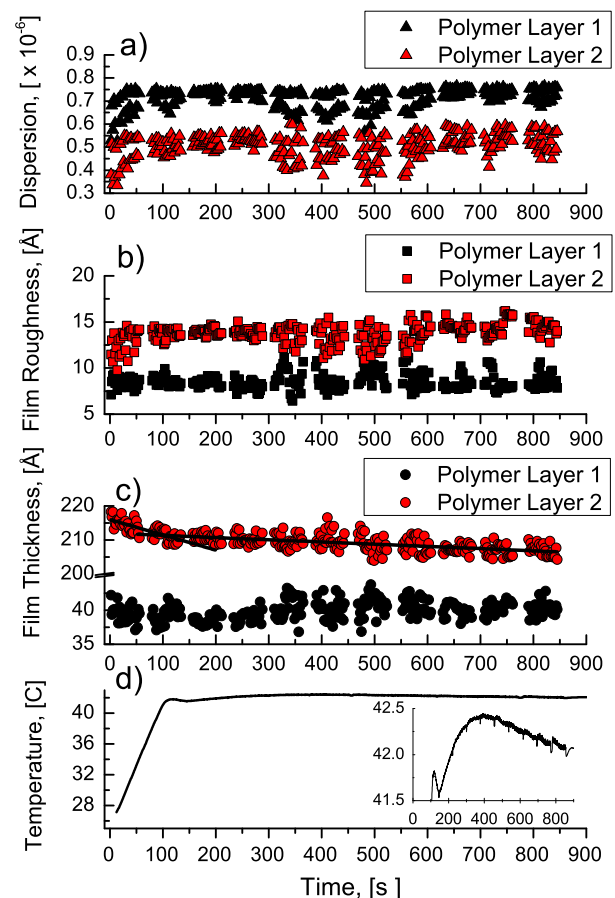


FIG. 5. Temperature vs. time curve (d) and temporal evolution of the parameters ((a)–(c)) describing the morphological changes of the polymer layer in our model. The temperature increased linearly from room temperature to over 42°C . The temperature exceeding of the set point (42°C) recorded for time > 200 s is pointed out in the “zoom in” box. The lines through the points in (c) highlight the two regimes described in the text.

it is obvious that at the start of the experiment both layers have lower dispersion values. With the increase of temperature (mainly in the linear regime), the dispersion values increase, i.e., the layers become denser (see Fig. 5(d)) which is in agreement with the coil-to-globule transformation that takes place at the hydrophilic/hydrophobic transition.

The values of all studied parameters significantly scatter between 300 s and 600 s. The scattering of the data coincides with temperatures above 42°C .

The dispersion data at the beginning of the experiment seem to exhibit two states. Up to now it is unclear, if this has a physical reason or it is related to the data frames connecting procedure as well as to the setup or the used model. However, the dispersion is taken as a measurement of the rest water in the polymer film,¹⁷ so it could be that the water transport mechanism is responsible for the observed two states in the beginning.

The work of Vidyasagar *et al.*¹⁷ supports the two layer model, and according to the authors the Poly1 layer has to be water rich and no water losses during the hydrophilic/hydrophobic transition. It would mean that the dispersion of the Poly1 has to be less than that of Poly2 and remains constant. In this work, we did not investigate different

models and emphasize on the fast reflectivity method itself. We believe that these few example experiments are not sufficient to properly access the ongoing discussion about the structure heterogeneity of thin polymer films in the film depth.

The effect of the hydrophilic/hydrophobic transition and reduction of the polymer film thickness are not as strong as reported in the literature^{15,16} since the current samples are not fully swollen after preparation. The samples are measured directly after the spin-coating and were heated in air. A sample environment chamber with humidity control was not available for this experiment. The spin-coated sample is almost dry and only the residual water from the film preparation is embedded in the polymer. Nevertheless, it should be mentioned that the method is sensible to the tiny film thickness changes caused by the temperature. Therefore, it could be successfully exploited to investigate the hydrophilic/hydrophobic transition in thin film and better understanding the constraining effect defined by the surface.

CONCLUSIONS

Our new approach for performing fast x-ray reflectivities already showed promising results. By offering a much better time resolution (down to a quarter of a second) this new method opens new opportunities for *in situ* reflectivity studies. Depending on the specimen under study, the q -range and the spatial resolution can be adapted. With photon energy in the range of 14–20 keV maximum q_z -values of 1 \AA^{-1} can be achieved. The spatial resolution mainly depends on the beam properties and the detector pixel size. The time resolution of the data acquisition depends on the speed of the rotation table, the photon flux, and the sample detector distance. In the study presented here, the reflectivity curves were recorded with a time resolution of 2 s; however, better time resolution can be achieved. The main challenges of the method are to cope with (1) the high flux in the forward direction and (2) the high scattering background which swamps the reflectivity at large q_z . A specially designed absorber was placed just in front of the detector to reduce the high flux in forward direction, which would saturate the detector. The background signal was suppressed by adjusting a knife-edge blade above the sample and recording a complete reflectivity curve based on several tens of frames with short exposure times (typically 0.05–0.1 s). The acquisition time turns out to be an important parameter to insure high quality of the data. A systematic study of the different experiment parameters such as the piezo rotation speed and the detector exposure time is foreseen. A better understanding of the influence of the parameters on the quality of the collected data would guide us to optimize the different parameters depending on the system under investigation and achieve better time resolution. Finally, it should be mentioned

that this setup can be easily designed as a stand-alone solution which would fit at almost every synchrotron beamline.

- ¹V. Holý, J. Kuběna, I. Ohlídal, K. Lischka, and W. Plotz, “X-ray reflection from rough layered systems,” *Phys. Rev. B* **47**, 15896 (1993).
- ²J. Als-Nielsen and D. McMorrow, *Elements of Modern X-ray Physics* (Wiley, New York, 2001).
- ³J. Daillant and A. Gibaud, *X-Ray and Neutron Reflectivity: Principles and Applications* (Springer, Berlin Heidelberg, 1999).
- ⁴M. Tolan, *X-Ray Scattering from Soft-Matter Thin Films* (Springer, Berlin Heidelberg, 1999).
- ⁵T. Hosokai, A. Gerlach, A. Hinderhofer, C. Frank, G. Ligorio, U. Heinemeyer, A. Vorobiev, and F. Schreiber, “Simultaneous *in situ* measurements of x-ray reflectivity and optical spectroscopy during organic semiconductor thin film growth,” *Appl. Phys. Lett.* **97**, 063301 (2010).
- ⁶N. Zotov, J. Feydet, A. Savan, A. Ludwigand, and J. von Borayny, “Interdiffusion in Fe/Pt multilayers: *In situ* high temperature synchrotron radiation reflectivity study,” *Adv. Eng. Mater.* **13**, 475 (2011).
- ⁷A. G. Richter and I. Kutzmenko, “Using *in situ* x-ray reflectivity to study protein adsorption on hydrophilic and hydrophobic surfaces: Benefits and limitation,” *Langmuir* **29**, 5167 (2013).
- ⁸G. Renaud, Y. Garreau, P. Betinelli, A. Tournieux, J. Bisou, P. Monteiro, and X. Elattaoui, “Beamline fast and automatic attenuation system for x-ray detectors at synchrotron soleil,” *J. Phys.: Conf. Ser.* **425**, 082003 (2013).
- ⁹C.-H. Lee, K.-L. Yu, and H.-C. Lee, “Study of the limitation of energy dispersive reflectivity with synchrotron radiation,” *Nucl. Instrum. Methods Phys. Res., Sect. A* **467–468**, 1073 (2001).
- ¹⁰T. H. Metzger, C. Luidl, U. Pietsch, and U. Vierl, “Novel versatile x-ray reflectometer for angle and energy dispersive characterization of liquid and solid surfaces and interfaces,” *Nucl. Instrum. Methods Phys. Res., Sect. A* **350**, 398 (1994).
- ¹¹S. Kowarik, A. Gerlach, W. Leitenberger, J. Hu, G. Witte, C. Wöll, U. Pietsch, and F. Schreiber, “Energy-dispersive x-ray reflectivity and GID for real-time growth studies of pentacene thin films,” *Thin Solid Films* **515**, 5606 (2007).
- ¹²U. Pietsch, J. Grenzer, T. Geue, F. Neissendorfer, G. Brezesinski, C. Symietz, H. Möhwald, and W. Gudat, “The energy-dispersive reflectometer at BESSY. II: A challenge for thin film analysis,” *Nucl. Instrum. Methods Phys. Res., Sect. A* **467–468**, 1077 (2001).
- ¹³A. Naudon, J. Chihab, P. Coudeau, and J. Mialut, “New apparatus for grazing x-ray reflectometry in the angle-resolved dispersive mode,” *J. Appl. Crystallogr.* **22**, 460 (1989).
- ¹⁴A. Meeents, S. Gutmann, A. Wagner, and C. Schulze-Briesse, “Origin and temperature dependence of radiation damage in biological samples at cryogenic temperatures,” *Proc. Natl. Acad. Sci.* **107**, 1094 (2010).
- ¹⁵W. Wang, E. Metwalli, J. Perlich, C. M. Papadakis, R. Cubitt, and P. Mueller-Buschbaum, “Cyclic switching of water storage in thin block copolymer films containing poly(*N*-isopropylacrylamide),” *Macromolecules* **42**, 9041 (2009).
- ¹⁶W. Wang, G. Kaune, J. Perlich, C. M. Papadakis, A. M. Bivigou Koumba, A. Laschewsky, K. Schlage, R. Roehlsberger, S. V. Roth, R. Cubitt, and P. Mueller-Buschbaum, “Swelling and switching kinetics of gold coated end-capped poly(*N*-isopropylacrylamide) thin films,” *Macromolecules* **43**, 2444 (2010).
- ¹⁷A. Vidyasagar, J. Majewski, and R. Toomey, “Temperature induced volume-phase transitions in surface-tethered poly(*N*-isopropylacrylamide) networks,” *Macromolecules* **41**, 919 (2008).
- ¹⁸J. A. Reed, S. A. Love, A. E. Lucero, C. L. Haynes, and H. E. Canavan, “Effect of polymer deposition method on thermoresponsive polymer films and resulting cellular behavior,” *Langmuir* **28**, 2281 (2012).
- ¹⁹O. H. Seeck, C. Deiter, K. Pflaum, F. Bertram, A. Beerlink, J. Horbach, H. Schulte-Schrepping, H. Franz, B. M. Murphy, M. Greve, and O. Magnussen, “The high-resolution diffraction beamline P08 at PETRA III,” *J. Synchrotron Radiat.* **19**, 30 (2012).